THE PROTEIN SOCIETY

Crystallographic evidence for two-metal-ion catalysis in human pol η

Jimin Wang* and Zachary B. Smithline

Department of Molecular Biophysics and Biochemistry, Yale University, New Haven, Connecticut, 06520

Received 20 August 2018; Accepted 2 October 2018
DOI: 10.1002/pro.3541
Published online 11 December 2018 proteinscience.org

Abstract: Extensive evidence exists that DNA polymerases use two metal ions to catalyze the phosphoryl transfer reaction. Recently, competing evidence emerged, suggesting that a third metal ion, known as MnC, may be involved in catalysis. The binding of MnC was observed in crystal structures of the replication complexes of human polymerase (pol) η, pol β, and pol μ. Its occupancy (q_{MnC}) in the pol η replication complexes exhibited a strong correlation with the occupancy of the formed product pyrophosphate (q_{PPi}), i.e., $q_{MnC} \propto q_{PPi}$. However, a key piece of information was missing that is needed to distinguish between two possible sequences of events: (i) the chemical reaction occurs first with only two meal ions, followed by the binding of MnC in a "catch-the-product" mode; and (ii) MnC binds first, followed by the chemical reaction with all three metal ions in a "push-the-reaction-forward" mode. Both mechanisms can lead to a strong correlation between q_{MnC} and q_{PPi}. However, $q_{MnC} \leq q_{PPi}$ in the first scenario, whereas $q_{MnC} \geq q_{PPi}$ in the second. In this study, an analysis of crystallographic data published recently for pol η complexes shows that the formation of the product pyrophosphate definitely precedes the binding of MnC. Therefore, just like all other DNA polymerases, human pol η employs a two-metal-ion catalytic mechanism. Rather than help to catalyze the reaction, MnC stabilizes the formed product, which remains trapped inside the crystals, before it slowly diffuses out.

Keywords: two-metal-ion catalysis; three-metal-ion catalysis; spherically averaged electron density function; saveED; polymerases; polymerization; pyrophosphorolysis

Introduction

Replication complexes of DNA polymerases (pols) in crystal structures have always been seen to contain two catalytic divalent metal ions, known as A (or MnA, MgA, or MeA) and B (MnB, MgB, or MeB).[1–7] The binding of a third metal ion, C (MnC, MgC, or MeC), was first discovered in 2012 in the crystal structure of the replication complex of human pol η in pH jump (6.0–7.0) experiments.[8] This system has already been studied in great detail with elaborate metal ion-substitution soaking experiments (i.e., Mn^{2+} or Mg^{2+} for Ca^{2+}) and time-lapse crystallography.[9] It has been shown that the occupancy of the third Mn^{2+} cation, q_{MnC}, bears a strong correlation with the occupancy or the fractional formation of the product pyrophosphate (PPi), q_{PPi}, i.e., $q_{MnC} \propto q_{PPi}$ (Fig. 1).[9]

Two competing hypotheses can explain the strong correlation observed: (i) MnC binds via thermal motion before the chemical step and assists in catalysis, i.e., it is part of the transition state (TS); and (ii) MnC binds immediately after the elemental chemical step to stabilize the formed product within the complex, but is not directly involved in catalysis. It is predicted that $q_{MnC} \geq q_{PPi}$ in the first scenario, but that $q_{MnC} \leq q_{PPi}$ in the second. These occupancies together represent the critical piece of causality information that is currently missing. In this study, we reanalyze crystallographic data recently published for pol η complexes, provide the missing causality

Additional Supporting Information may be found in the online version of this article.

Grant sponsor: National Institutes of Health GM022778.

*Correspondence to: Jimin Wang, Department of Molecular Biophysics and Biochemistry, Yale University, New Haven, CT 06520. E-mail: jimin.wang@yale.edu

This study is dedicated to Professor Thomas A. Steitz, our mentor and long-time colleague.

information, and resolve the functional ambiguity of MnC.

Metal ion C has since been seen in human pol β and pol μ as well.[10,11] A difference between pol η and the latter two pols is that PPi appears to be trapped in the pol η replication complex whereas it slowly diffuses out of the crystals in the latter two. As a result, there is no apparent correlation between q_{MnC} and q_{PPi} in either pol β or pol μ, and q_{MnC} appears always smaller than q_{PPi}, which implies that, in these pols, catalysis proceeds with only the first two metal ions, A (the catalytic metal ion) and B (the nucleotide-binding metal ion).[12] The binding of divalent metal ion C (the product metal ion) does not appear to lower the activation barrier of the TS of pol β according to density functional theory calculations.[13,14] Therefore, any direct involvement of this metal ion in catalysis in these two pols has been ruled out.[13,14]

Materials, methods, and crystallographic theory

When atomic electron density (ED) peaks in the experimental data (like those of the metal ions in question) are fully resolved in the pol η replication complexes (Fig. 1), they can be spherically averaged as a function of radial distance. A function that performs such a task, which we called saveED, or spherically averaged ED, is determined by both random atomic displacements (or atomic B-factor, $B = 8\pi^2\langle\Delta r\rangle^2$) and occupancy ($q$). It obeys the following equations[15,16]:

$$\rho(r,B,q) = q\int f d\tau = 8\pi^{3/2} q \sum_{j=1}^{5} \frac{a_j e^{-4\pi^2 r^2/(b_j+B)}}{(b_j+B)^{3/2}}. \quad (1)$$

$$\rho(r,B,q)/\rho(0,B,q) = \sum_{j=1}^{5} \frac{a_j e^{-4\pi^2 r^2/(b_j+B)}}{(b_j+B)^{3/2}} \Big/ \sum_{j=1}^{5} \frac{a_j}{(b_j+B)^{3/2}}. \quad (2)$$

In these equations, a_j and b_j are Gaussian function-fitted parameters of atomic scattering factors. Equation 2 is only dependent on B, but not on q, so q and B can be completely decoupled and determined accurately for any given metal ion of interest. When B is large, or is made to be so after-the-fact through B-blurring, i.e., $B >> b_j$ and $B + b_j \approx B$, the four Gaussian functions in the above equations can be approximated with a single Gaussian function:

$$\rho(r,B,q) = q\int f d\tau \approx 8\pi^{3/2} q \sum_{j=1}^{5} \frac{a_j e^{-4\pi^2 r^2/B}}{(B)^{3/2}} = \left[8\pi^{3/2} q Z B^{-1.5}\right] e^{-4\pi^2 r^2/B}. \quad (3)$$

$$ln[\rho(r,B,q)/\rho(0,B,q)] = -\left[4\pi^2/B\right] r^2. \quad (4)$$

In Equation 3, Z is the sum of five a_j coefficients, which represents the Z value of a neutral element or the total number of electrons for an ionized atom. When an internal reference is used, any small difference in B value between a query and the reference can be minimized and removed, using a least-squares procedure according to the linear equation of a logarithmic plot against the radial distance squared, as outlined in Equation 4. Once this B-factor difference is removed, the relative occupancy can be determined using another least-squares procedure for a linear equation outlined in either (1) or (3).

ED functions reported for human pol η structures were Fourier synthesized at any given position from corresponding σ_A-weighted $2F_{obs}–F_{calc}$ coefficients, including an estimated F(000) term. Coordinates were sampled at 12 points, arranged with cuboctahedral symmetry on the surface of a sphere with a radius increment of 0.01 Å, and corresponding ED values were averaged (i.e., saveED). Fourier coefficients were obtained from the coordinates retrieved from the PDB using the program[17] Refmac5 by setting the refinement cycle to zero. Although the PDB ID codes for the 91 structures reported for human pol η were left as blanks, at least 36 entries could be found through a relationship to the single known entry, 4ECV, described in that paper.[9] All of these available entries were retrieved for analysis on the basis of header information provided in the PDB files. Relevant PDB entries used in this study are given in Table I.

Results

Occupancies of the metal ions in the replication complex of human pol η

Equations 1–4 reveal that the ED peak value $\rho(0,B,q)$ depends on the B-factor to the power of −1.5 whereas it depends linearly on occupancy q. When B-factors are different, q does not always bear a linear relationship with the peak of the ED function or of the difference ED function. When q is overestimated, model refinement increases the B value for compensation, and when q is underestimated, model refinement decreases the B value. Therefore, the occupancies previously reported using standard model refinement procedures could have very large uncertainties.[9] This problem is completely resolved here using saveED functions.

Different B-factors for Mn^{2+} ions at different time points can be readily seen from (i) B-factors refined in the coordinate files, (ii) raw saveED plots, and (iii) different shapes of ED at given contouring levels (Figs. 1 and 2). By contrast, on the basis of the peak size in the F_{obs}(600s)–F_{obs}(30s) difference Fourier map, one cannot distinguish whether large peaks observed between the two data sets at the A, B, and C sites are contributed by either changing q, B, or both, [Fig. 1(e,f)]. In addition, subtle structural changes occur within the entire DNA duplex upon product formation, which can also complicate the analysis [Fig. 1(f)].

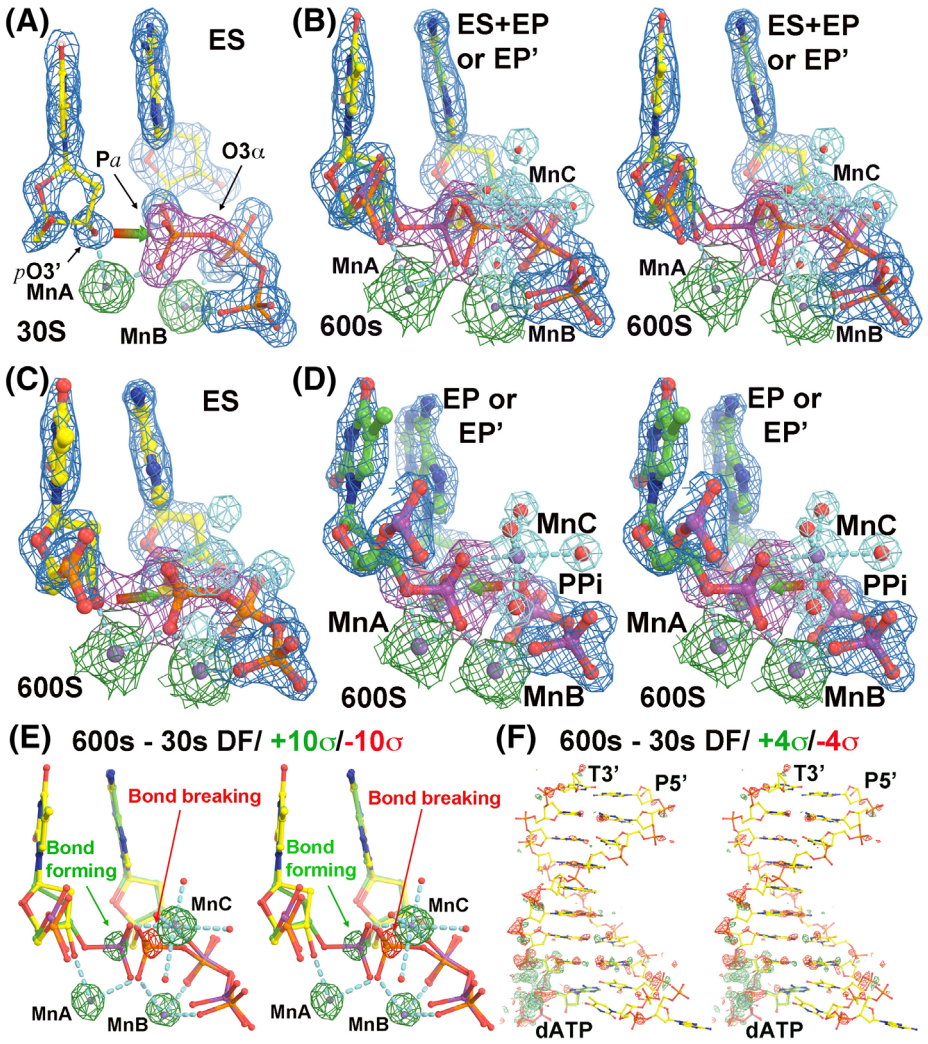

Figure 1. The structures of human pol η replication complexes. (a) The enzyme–substrate (ES) complex at 30s. Red-green arrow shows the direction of nucleophilic attack by primer-terminus O3' (*pt*O3') to α-phosphorus atom of incoming dATP. MnC does not bind in the ES complex. (b) Stereodiagram of a mixture of the ES complex with the enzyme-product (EP or EP') complex at 600s. (c) The ES complex at 600s. (d) Stereodiagram of the EP or EP' complex at 600s. Red-green arrow shows the direction of pyrophosphorolysis. The σ_A-weighted $2F_{obs}$–F_{calc} maps in panels (a–d) are contoured at 2σ, but shapes of atomic ED functions of MgA and MgB are quite different at this same contouring level. (e, f) Stereodiagrams of F_{obs}(600s)–F_{obs}(30s) difference Fourier maps contoured at ±10σ (green and red) and ± 4σ for the catalytic site (e) and for the entire DNA duplex (f).

The raw saveED functions obtained for MnC, MnA, and MnB differ at all five time points within each data set, as well as among individual data sets in the presence of 10 mM [Mn^{2+}] soaking, where metal ion peaks are reasonably well resolved [Fig. 2(a–c)]. For each data set, curves for both MnC and MnB can be fitted to that of MnA [Fig. 2(d) and Table I]. In fact, all curves of Mn^{2+} centers can be fitted to each other with only subtle differences between the MnC curve and those of the other two metal ions, when r < 1 Å [Fig. S1(a)]. The results show that q_{Mnc} remains largely unchanged from 90 to 300 s and increases rapidly at 600 s, whereas q_{MnB} is nearly saturated at all time points (Table I).

An analysis of saveED for the structures in the presence of 1 mM [Mn^{2+}] as well as the fitted occupancies at all five time points (PDB-ID, 5kfb, 5kfc, 5kfd, 5kfe, and 5kff) shows that $q_{MeB} > q_{MeA}$ (Fig. S3), which is opposite the results observed for the longer time points at 10 mM (Table I) and the estimates reported previously[9] [Fig. 3(f)].

The root-mean-square difference (rmsD) of fitted occupancies is 2%, between two sets of fittings; one set was obtained using an internal reference within each

Table I. *Estimated Occupancies of MnB, MnC, and PPi*

PDB ID (time point)	Reference MnA	MnB	MnC	PPi
5kfh (90s)	1.00	0.87	0.30	0.35
5kfi (120s)	1.00	0.92	0.34	0.39
5kfj (180s)	1.00	0.97	0.30	0.42
5kfk (300s)	1.00	1.01	0.36	0.51
5kfl (600s)	1.00	1.04	0.52	0.57

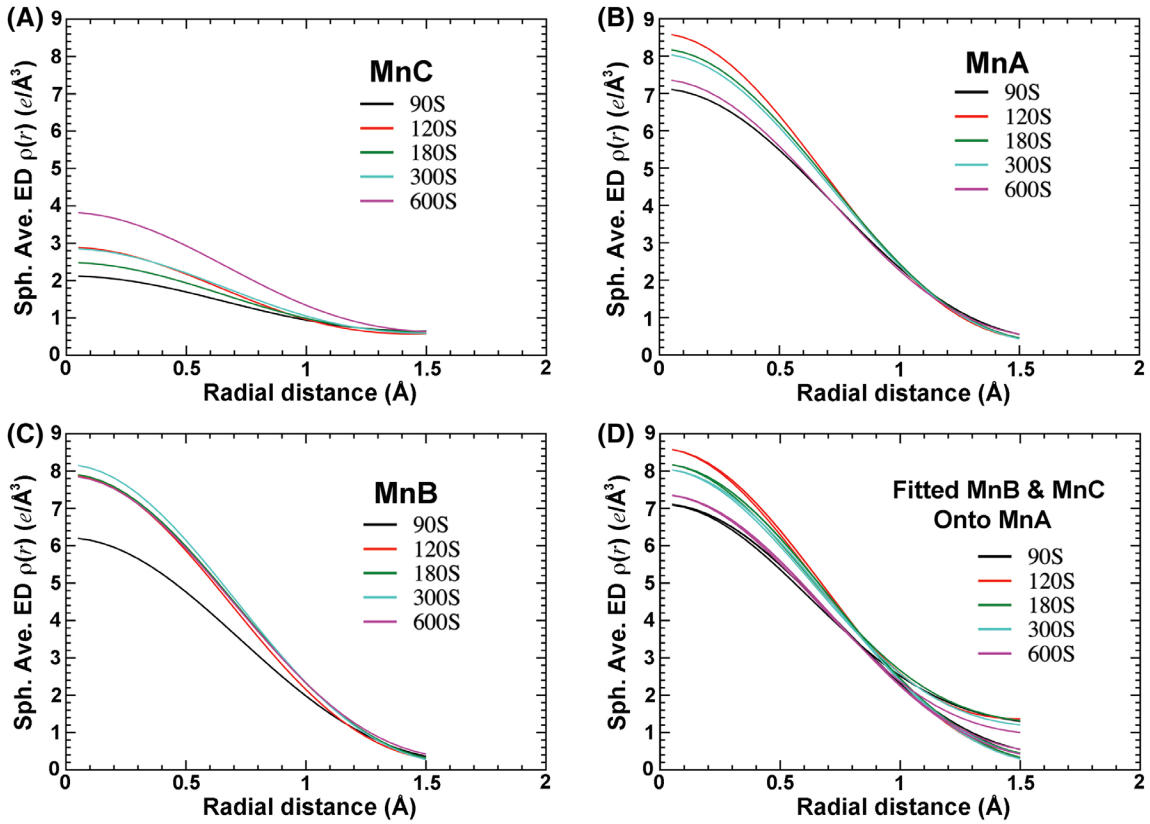

Figure 2. Spherically averaged ED functions (saveED) at five time points. (a) MnC. (b) MnA. (c) MnB. (d) Fitted MnB and MnC curves onto that of MnA for each data set. See Fig. S1A for fitting of all curves onto a single common reference curve.

data set, and the second set done using a single reference for all the data sets. This rmsD value represents an estimated error for the q values determined. It lies within the expectation because the binding of MnC involves an increase of 23e at its full occupancy.

Occupancy of PPi

The percentage of bond formation between the primer terminus O3' (*pt*O3') and the α-phosphorus (Pα) of the incoming dATP can be seen as an increasing ED feature at the midpoint between these atoms [Fig. 1(e)]. The actual bond formation is invisible in ED maps obtained using X-ray crystallography when neutral atomic scattering factors are used in model refinement (see below). However, upon bond formation and breakage, the phosphorus center is displaced from the substrate side to the product side, which results in symmetric pairs of positive and negative peaks [Fig. 1 (e)]. The heights of these symmetric peaks are proportional to both bond formation and bond breakage.

The percentage of bond breakage between Pα and O3α can be seen as a decreasing ED feature at the midpoint between these atoms [Fig. 1(e)]. The three atoms *pt*O3', Pα, and O3α are approximately collinear, so the changing ED features as a function of time can be visualized in a one-dimensional ED plot along the axis connecting all three atoms [Fig. 3(a)]. The maximal ED gain or loss is plotted as a function of time point and normalized in a fractional unit [Fig. 3(b,c)]. The product formation appears to monotonically increase with the time from 90 to 600 s [Fig. 3(d)].

The occupancy of MnC is always lower than that of the formed PPi

When q_{MnC} and q_{PPi} are compared, the two quantities indeed bear a strong correlation as previously observed.[9] However, q_{MnC} is always smaller than q_{PPi}, by as much as eight times the estimated error, for all five time points analyzed [Fig. 3(d) and Table I]. This observation suggests that the binding of MnC always trails behind product formation, i.e., MnC binds only to the already formed PPi after the chemical step, not before it. Therefore, MnC does not bind the enzyme–substrate (ES) complex prior to the TS and before the chemical step. It binds only to the already formed enzyme–product (EP) complex after catalysis, resulting in a new type of MnC-bound EP complex, which we here call EP' (Fig. 1). The concentration of MnC-bound product represents only part of the total amount of product. Thus, it is always true that [MnC] = [EP'] < [EP'] + [EP].

Discussion

Accuracy of occupancy determination

There indeed exists a strong correlation between q_{MnC} and q_{PPi}, as reported previously.[9] However, the exact

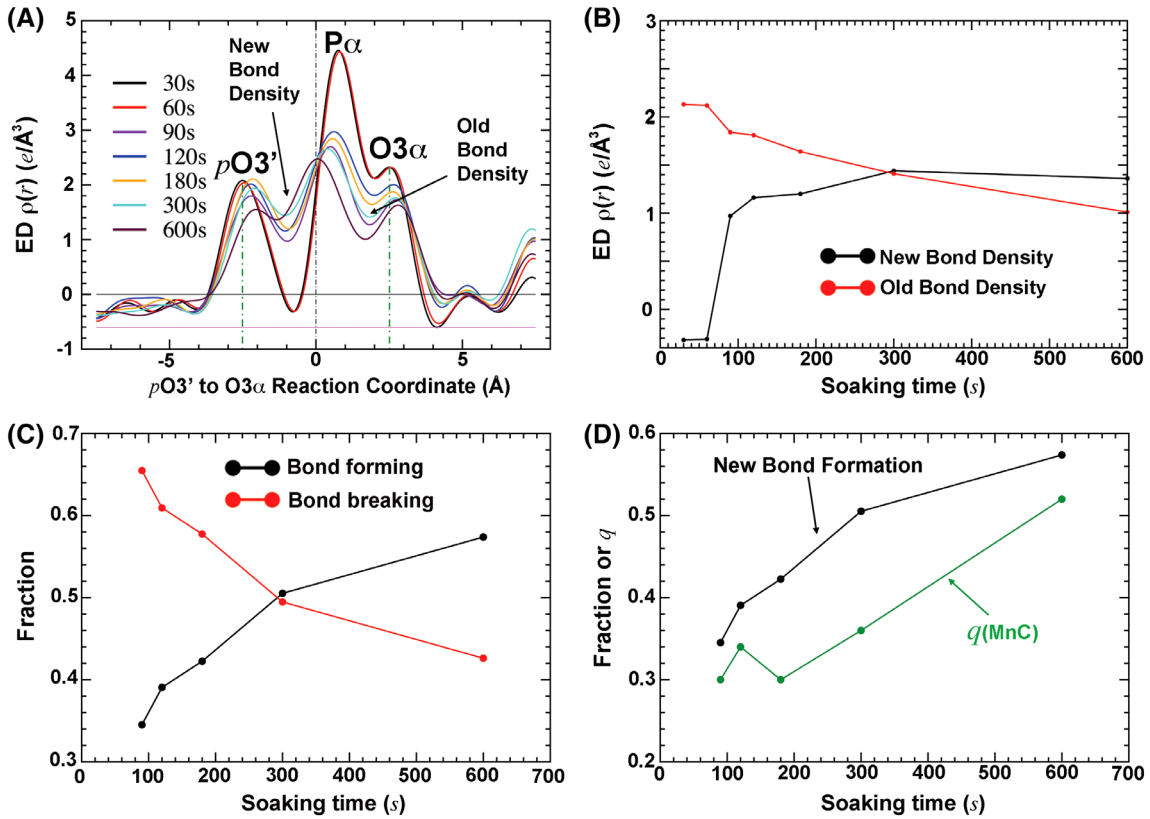

Figure 3. Bond formation and bond breakage. (a) One-dimensional ED plot along the reaction coordinate. (b) New and old bond densities as a function of time. (c) Normalized fraction of bond formation and bond breakage. (d) Comparison of q_{PPi} and q_{MnC} obtained. See Fig. 1(B) for logarithmic time plot, which shows the single-exponential curve for the bond formation.

occupancies obtained in this analysis, most notably q_{MnC}, differ from those estimated previously. The binding of new MnC results in very large difference ED features because it leads to a total of 23*e* at its full occupancy. Even when $q_{MnC} \sim 0.30$ (0.7*e*), the MnC signal is still larger than a change of valence electrons associated with new bond formation. According to the negative Laplacian relief plot of the charge density function, the transferred valence electrons are largely spherically symmetrically distributed in outer shells with only a small fraction of the total valence electrons that actually contribute to the so-called deformation ED enriched between two bonded atoms.[18] The deformation ED is the difference between the actual experimental ED function and the calculated ED function using spherical atomic scattering factors; it is observable only at sub-Å resolution in X-ray crystallography.[18] The charge density function is derived from the electrostatic potential function using another negative Laplacian operation according to the Poisson equation.[15]

Previously,[9] q_{MnC} was substantially overestimated on the basis of the heights of F_{obs}–F_{calc} difference Fourier peaks without proper spatial integration or calibration of the expected 23*e* for Mn^{2+} at its full occupancy (here, F_{calc} represents the calculated amplitudes from an atomic model before MnC was built). An overestimated q_{MnC} would support a new catalytic mechanism involving three metal ions.[9]

It should be noted that in this study, the baseline of ED functions appears below zero [Fig. 3(a)]. This is likely attributable to (i) model phase errors and (ii) missing reflections at resolutions <20 Å and >1.55 Å, (see PDB-ID 5KFG)[9], because $\langle I/\sigma_I \rangle$ = 3.3 in the highest resolution shell is too large, which would introduce significant effects from Fourier series termination.[15] In our study, we better accounted for these effects by using an internal reference [properly estimated F(0,0,0) has already been included in our calculations]. Had these steps not been properly taken, the absolute occupancies determined could have been highly inaccurate. However, the accuracy of relative order of the occupancies should not be affected as much.

It is likely that the quality of all atomic models of pol η replication complexes[9] can be further improved when all significant peaks in the residual F_{obs}–F_{calc} maps are properly explained.[19] (The free *R*-factors of the current model are ~ 20% to 22% at resolution of ~ 1.55 Å.) However, when an F_{obs}(1800s/1mM/Mn^{2+})–F_{obs}(90s/1mM/Mn^{2+}) difference Fourier map was calculated, peaks corresponding to the product formed and the binding of MnC were indeed detectable at 1 mM Mn^{2+} at the 1800 s time point,

but were unable to be quantified (only $\sim 3.6\sigma$ for MnC; this is very small, and thus the data are not shown). Of course, the F_{obs}(1800s/1mM/Mn^{2+})–F_{obs} (90s/1mM/Mn^{2+}) difference map with an overall isomorphous *R*-factor value of 10.4% between the two data sets is far more sensitive than the corresponding F_{obs}–F_{calc} map given the current model free *R*-factor values of 20.7–22.2% (Fig. S2).

The mode of metal ion C binding in the enzyme-product complex

According to quantum mechanical calculations,[20] the coordination energy of an octahedral $[Mg(II)(H_2O)_6]^{2+}$ complex ion is dominated by Coulombic energy involving charges or atomic partial charges in which O has $-0.78e$, H has $+0.39e$, and Mg(II) has $+2.00e$, with a mean coordination bond length of 2.08 Å. The shortest O–O distance in the Mg(II) complex ion is $\sim$ 2.94 Å whereas the O–O distance within each phosphate group is $\sim$ 2.5 Å. For this reason, Mg^{2+} cannot bind at the MgC site to simultaneously ligate two O atoms of the same phosphate group in the ES complex. Even when one water molecule ligand of the $[Mg(II)(H_2O)_6]^{2+}$ complex is replaced with a hydroxyl anion after deprotonation, its coordination bond length is reduced only slightly to 2.03 Å. The shortest O–O distance is still greater than 2.87 Å, which is longer than the O–O distance within each phosphate. For this reason, Mg^{2+} cannot bind dNTP or any phosphate group in the coordination configuration of circular 4-atom connectivity under any circumstance. However, this configuration differs from that of MgB bound to the triphosphate moiety of the incoming dATP, which has circular 6-atom connectivity. Moreover, Mg^{2+} does not bind any bridging O atom because such an O atom has a significantly reduced atomic partial charge relative to non-bridging O atoms.

The observed binding mode of MnC to the two products, i.e., the PPi and the newly formed phosphodiester that are no longer covalently connected, is not subject to the geometric constraints of connectivity just discussed. Because the binding of MnC does not directly involve any group of human pol η, its stability is solely determined by both the geometry of products (or substrate, if such binding is ever possible) and atomic partial charges of potential ligands. The binding of MnC can only occur after the formation of PPi, whose O2 atom carries a $-1e$ charge.

Because MnC binds the EP complex but not the ES complex, it would be very difficult to extrapolate whether it can bind the TS. If one takes the geometry of the $[MgF_3]^-$ complex ion that binds the phosphorane site to mimic the TS for the phosphoryl transfer reaction,[21] the F-O distance is $\sim$ 2.80 Å, which is still shorter than the O–O distance of the preferred Mg(II) complex ions.[20] This implies that direct binding of MgC at the TS would require energetic compensation. Therefore, the binding of MgC does not stabilize the TS and does not contribute to catalysis. A similar geometric analysis of the TS coordination involving both Mg^{2+} and Mn^{2+} in the replication complex of bacteriophage RB69 DNA pol (RB69pol) has already been discussed elsewhere.[22] The finding of this analysis is also fully consistent with density functional theory studies done recently on human pol η, pol β, and pol η, which suggest that MgC cannot support the phosphorolysis reaction.[12–14,23] By the micro-reversibility property of TS theory,[24] MgC cannot support the polymerization reaction, either.

With the exception of high-oxidation Mn(III) and Mn(IV) ions, as found[25,26] in photosystem II (where the Mn-O bond for μ-O bridge can be reduced to as short as 1.80 Å), typical Mn(II)-O coordination bond lengths are similar to that of the Mg-O bond within the $[Mg(II)(H_2O)_6]^{2+}$ complex ion.[20] The ionic radius of Mg^{2+} in octahedral coordination is 0.72 Å. The ionic radius of Mn^{2+} in high-spin octahedral coordination is 0.80 Å, and it is 0.67 Å in low-spin octahedral coordination, when ligands have large negative partial charges. With its known coordination properties, MnC can bind only *two* products of the already-formed EP complex, but cannot bind to the ES complex or to the TS structure.

Two-metal-ion catalytic mechanism

Only two metal ions, MeA and MeB, bind to both the ES complex and the EP complex, from which complexes the TS structure has been extrapolated for both human pol β and RB69pol.[22,27] The catalytic MgA encounters the same problem as discussed above, a coordination configuration of cyclic 4-atom connectivity. However, the situation is resolved in the TS structure because two substrate ligands to MgA have a full negative charge. The *pt*O3' group is deprotonated at the TS and bears a $-1e$ charge. Indirect evidence exists that R_p O atom of dNTP also has $-1e$ charge (due to polarization) because either its S_p O atom or the leaving PPi would have no net charge after protonation. This protonation occurs by a conserved Lys side chain during the two-proton transfer process in all DNA and RNA dependent DNA and RNA polymerases.[28,29] With two negative charges on two ligands in the two substrates at the TS, MgA carries out catalysis.

Reduced exchange rate with reduced [Mn^{2+}] requires longer time for catalysis

Assuming that the exchange rate of Mn^{2+} for pre-bound Ca^{2+} at all sites in pol η replication complex crystals is a first-order process, it should have been linearly proportional to free [Mn^{2+}] in the soaking solution. The net exchange at each site should have been reduced by 10 fold when [Mn^{2+}] was reduced by 10-fold from 10 m*M* to 1 m*M*. Assuming that the exchange rates in the metal ion A and B sites are independent, the concentration of the ES complex

containing both MnA and MnB substituted simultaneously would be reduced by 100-fold at 1 m*M* [Mn^{2+}] relative to 10 m*M* [Mn^{2+}] at any given time point. Using this relationship, the effective [ES] containing both MnA and MnB at the 1800 s time point and at 1 m*M* [Mn^{2+}] would be equivalent to that at 18 s and 10 m*M*. At the latter time point both [EP] and [EP'] are too low to be accurately quantified. An F_{obs}(1800s/1mM/Mn^{2+}) - F_{obs}(90s/1mM/Mn^{2+}) difference Fourier map indeed shows that a very low fraction of the total products [EP'] + [EP] was detectable on the basis of small peaks at the expected positions. At early time points ≤ 60s at 10 m*M* [Mn^{2+}], it is much easier to detect the product-bound MnC (a difference of total 23*e*) than the formed product itself. Therefore, the lack of significant product formation in the presence of 1 m*M* [Mn^{2+}] is likely due to too short a reaction time, not the fact that two metal ions failed to catalyze the polymerization reaction as hypothesized previously.[9]

An analysis of saveED for the structures in the presence of 1 m*M* [Mn^{2+}] suggests possible complex exchange sequences of metal ions A and B, which were known previously in RB69 to involve transient re-opening of the fingers domain.[30,31] In early stages of metal ion exchange, relative metal ion occupancies are determined by accessibility (i.e., forward kinetics), but in later stages, they are determined by relative stability (i.e., thermodynamics, or both forward and backward kinetics). Metal ion exchange kinetics in crystal shows that $q_{MeB} > q_{MeA}$ in pol η replication complexes (Fig. S3), which is as complicated as in solution.

Other crystallographic evidence for a two-metal-ion mechanism

Aside from the q_{MnC} vs q_{PPi} relationship just described, all existing crystallographic and kinetic data reported[9] for human pol η appear largely consistent with the two-metal-ion mechanism, or can be reasonably explained by it. For example, if MgC were indeed part of the TS, substitution of S for O at the S_p position of the α-phosphate of dATP, which is a ligand only to MgC (or MnC) (Fig. 1), would completely abolish Mg^{2+} dependent catalysis if the chemical step is rate-limiting. The lost activity would be fully rescued by Mn^{2+} according to the well-established method of nucleotide analog interference mapping (NAIM).[32–34] Yet, the kinetic parameter k_{cat} for human pol η in solution increased over 2-fold for S_p-dATPαS relative to dATP (which is also known as thio-elemental effect) regardless of whether Mg^{2+} or Mn^{2+} was used.[9] Moreover, MgC was not observed to bind in crystal structures under any condition when S_p-dATPαS was a substrate.[9] These observations completely rule out the involvement of metal ion C in catalysis by human pol η.

Consistent with the well-established theory of NAIM,[32–34] human pol β Mg^{2+}/S_p-dATPαS over Mg^{2+}/R_p-dATPαS increases by 57.5-fold (which is known as stereoselectivity) because Mg^{2+} does not interact well with the thio group at the R_p position.[35] This preference is largely erased when Mn^{2+} is used as a cofactor, i.e., Mn^{2+} has rescued the lost activity because Mn^{2+} binds well to the substituted thio group.[35] Stereoselectivity in general is much greater than thio-elemental effects among all DNA polymerases that have been carefully examined.[35–39]

The increased k_{cat} for the substrate S_p-dATPαS and the lost binding of MeC in the replication complexes of human pol η (Ref. 9) suggest that the binding of MeC may promote the reverse reaction by retaining the PPi in the replication complex longer, and thus may actually inhibit the overall polymerization reaction. Inhibitory effects of excess free metal ions in solution have been studied for a number of DNA pols, but not for human pol η. For example, free [Mg^{2+}] ≥ 10 m*M* in solution begins to inhibit the polymerization reaction catalyzed by RB69pol in a systematic analysis of an [Mg^{2+}]-dependent activity profile,[30] a property shared with its cousin, bacteriophage T4 DNA pol.[40] Similarly, free [Mg^{2+}] in solution (after excluding those already in the complex with metal-ion-exchange-inert Rh(III) dNTP) required for the polymerization reaction catalyzed by human pol β and *Escherichia coli* DNA pol I is typically in the low micro-molar range.[41,42] Given that equivalent studies have not yet been done for human pol η, the corresponding inhibitory concentrations of Mg^{2+} and Mn^{2+} remain unknown, and it remains to be determined whether the binding of MeC corresponds to the metal ion-inhibited complex.

The existing crystallographic and kinetic data[9] obtained for the R61A mutant of human pol η further support the hypothesis that MeC is not involved in catalysis in this enzyme. MeC binds four water molecules plus a weak ligand from the newly-formed phosphodiester group, which has a much-reduced negative partial atomic charge, and another strong ligand from negatively charged PPi, which interacts with the R61 side chain in the ES complex of the wild type enzyme (Fig. 1). This side chain was displaced from the metal ion in the EP complex. It is therefore predicted that if MnC were part of the TS, the substitution of R61 with alanine would remove the energetic barrier for MnC to bind, the catalytic efficiency of this mutant enzyme would increase relative to that of the wild type enzyme, and thus rate of product formation would increase. Yet, the reverse was observed: the kinetic parameter k_{cat} of this mutant in solution was reduced by 3-fold relative to the wild type enzyme regardless of whether Mg^{2+} or Mn^{2+} was used as a cofactor.[9] Consistent with its solution kinetic data, the formation of products as well as the binding of MeC in this mutant complex was delayed by an extra 120 s relative to the wild type complex in crystals.[9] Thus, MnC can only bind to the already formed EP complex, but not to the ES complex or to the TS in human pol η.

Conclusions

Above, we resolved the order of events involving product formation and binding of metal ion C in human pol η replication complexes. MnC binds to the already-formed EP complex, not to the TS structure or the ES complex. Like in human pol β and pol μ, metal ion C stabilizes the product PPi, and is not involved in catalysis.

Acknowledgments

This work was supported in part by National Institutes of Health Grants P01 GM022778. The authors thank Dr W. H. Konigsberg for commenting on this manuscript.

REFERENCES

1. Pelletier H, Sawaya MR, Kumar A, Wilson SH, Kraut J (1994) Structures of ternary complexes of rat DNA-polymerase-beta, a DNA template-primer, and ddCTP. Science 264:1891–1903.
2. Doublie S, Ellenberger T (1998) The mechanism of action of T7 DNA polymerase. Curr Opin Struct Biol 8: 704–712.
3. Huang HF, Chopra R, Verdine GL, Harrison SC (1998) Structure of a covalently trapped catalytic complex of HIV-I reverse transcriptase: implications for drug resistance. Science 282:1669–1675.
4. Franklin MC, Wang JM, Steitz TA (2001) Structure of the replicating complex of a pol alpha family DNA polymerase. Cell 105:657–667.
5. Doublie S, Tabor S, Long AM, Richardson CC, Ellenberger T (1998) Crystal structure of a bacteriophage T7 DNA replication complex at 2.2 ångstrom resolution. Nature 391:251–258.
6. Yang W, Lee JY, Nowotny M (2006) Making and breaking nucleic acids: Two-Mg^{2+}-ion catalysis and substrate specificity. Mol Cell 22:5–13.
7. Steitz TA (2006) Visualizing polynucleotide polymerase machines at work. EMBO J 25:3458–3468.
8. Nakamura T, Zhao Y, Yamagata Y, Hua YJ, Yang W (2012) Watching DNA polymerase eta make a phosphodiester bond. Nature 487:196–U177.
9. Gao Y, Yang W (2016) Capture of a third Mg^{2+} is essential for catalyzing DNA synthesis. Science 352: 1334–1337.
10. Freudenthal BD, Beard WA, Shock DD, Wilson SH (2013) Observing a DNA polymerase choose right from wrong. Cell 154:157–168.
11. Jamsen JA, Beard WA, Pedersen LC, Shock DD, Moon AF, Krahn JM, Bebenek K, Kunkel TA, Wilson SH (2017) Time-lapse crystallography snapshots of a double-strand break repair polymerase in action. Nature Comm 8:253.
12. Perera L, Beard WA, Pedersen LG, Wilson SH (2017) Hiding in plain sight: The bimetallic magnesium covalent bond in enzyme active sites. Inorg Chem 56: 313–320.
13. Perera L, Freudenthal BD, Beard WA, Pedersen LG, Wilson SH (2017) Revealing the role of the product metal in DNA polymerase beta catalysis. Nucleic Acids Res 45:2736–2745.
14. Perera L, Freudenthal BD, Beard WA, Shock DD, Pedersen LG, Wilson SH (2015) Requirement for transient metal ions revealed through computational analysis for DNA polymerase going in reverse. Proc Natl Acad Sci USA 112:E5228–E5236.
15. Wang J (2018) Determination of chemical identity and occupancy from experimental density maps. Protein Sci 27:411–420.
16. Moore P. *Visualizing the invisible: imaging techniques for the structural biologist*. Oxford; New York: Oxford University Press, 2012.
17. Murshudov GN, Vagin AA, Dodson EJ (1997) Refinement of macromolecular structures by the maximum-likelihood method. Acta Cryst D53:240–255.
18. Koritsanszky T, Flaig R, Zobel D, Krane H, Morgenroth W, Luger P (1998) Accurate experimental electronic properties of DL-proline monohydrate obtained within 1 day. Science 279:356–358.
19. Wang J (2017) Systematic analysis of residual density suggests that a major limitation in well-refined X-ray structures of proteins is the omission of ordered solvent. Protein Sci 26:1012–1023.
20. Pavlov M, Siegbahn PEM, Sandstrom M (1998) Hydration of beryllium, magnesium, calcium, and zinc ions using density functional theory. J Phys Chem A 102:219–228.
21. Lahiri SD, Zhang G, Dunaway-Mariano D, Allen KN (2003) The pentacovalent phosphorus intermediate of a phosphoryl transfer reaction. Science 299:2067–2071.
22. Xia S, Wang M, Blaha G, Konigsberg WH, Wang J (2011) Structural insights into complete metal ion coordination from ternary complexes of B family RB69 DNA polymerase. Biochemistry 50:9114–9124.
23. Yoon H, Warshel A (2017) Simulating the fidelity and the three Mg mechanism of pol and clarifying the validity of transition state theory in enzyme catalysis. Proteins 85:1446–1453.
24. Kraut J (1988) How do enzymes work. Science 242: 533–540.
25. Wang J, Askerka M, Brudvig GW, Batista VS (2017) Insights into photosystem II from isomorphous difference Fourier maps of femtosecond X-ray diffraction data and quantum mechanics/molecular mechanics structural models. ACS Energy Lett 2:397–407.
26. Askerka M, Brudvig GW, Batista VS (2017) The O_2-evolving complex of photosystem II: recent insights from Quantum Mechanics/Molecular Mechanics (QM/MM), Extended X-ray Absorption Fine Structure (EXAFS), and femtosecond X-ray crystallography data. Acc Chem Res 50:41–48.
27. Batra VK, Beard WA, Shock DD, Krahn JM, Pedersen LC, Wilson SH (2006) Magnesium-induced assembly of a complete DNA polymerase catalytic complex. Structure 14:757–766.
28. Castro C, Smidansky E, Maksimchuk KR, Arnold JJ, Korneeva VS, Gotte M, Konigsberg W, Cameron CE (2007) Two proton transfers in the transition state for nucleotidyl transfer catalyzed by RNA- and DNA-dependent RNA and DNA polyrnerases. Proc Natl Acad Sci USA 104:4267–4272.
29. Castro C, Smidansky ED, Arnold JJ, Maksimchuk KR, Moustafa I, Uchida A, Gotte M, Konigsberg W, Cameron CE (2009) Nucleic acid polymerases use a general acid for nucleotidyl transfer. Nat Struct Mol Biol 16:212–218.
30. Lee HR, Wang M, Konigsberg W (2009) The reopening rate of the fingers domain Is a determinant of base selectivity for RB69 DNA polymerase. Biochemistry 48: 2087–2098.
31. Wang M, Lee HR, Konigsberg W (2009) Effect of A and B metal ion site occupancy on conformational changes in an RB69 DNA polymerase ternary complex. Biochemistry 48:2075–2086.
32. Ryder SP, Strobel SA (1999) Nucleotide analog interference mapping. Methods 18:38–50.

33. Suydam IT, Strobel SA (2009) Nucleotide analog interference mapping. Methods in Enzymology, Vol 468: Biophysical, Chemical, and Functional Probes of RNA Structure, Interactions and Folding, Part A. Methods in Enzymology 468:3–30.
34. Basu S, Morris MJ, Pazsint C (2012) Analysis of catalytic RNA structure and function by nucleotide analog interference mapping. Methods Mol Biol 848:275–296.
35. Liu J, Tsai MD (2001) DNA polymerase beta: pre-steady-state kinetic analyses of dATP-alpha-S stereoselectivity and alteration of the stereoselectivity by various metal ions and by site-directed mutagenesis. Biochemistry 40:9014–9022.
36. Kuchta RD, Mizrahi V, Benkovic PA, Johnson KA, Benkovic SJ (1987) Kinetic mechanism of DNA-polymerase-I (Klenow). Biochemistry 26:8410–8417.
37. Capson TL, Peliska JA, Kaboord BF, Frey MW, Lively C, Dahlberg M, Benkovic SJ (1992) Kinetic characterization of the polymerase and exonuclease activities of the gene-43 protein of bacteriophage T4. Biochemistry 31:10984–10994.
38. Patel SS, Wong I, Johnson KA (1991) Pre-steady-state kinetic-analysis of processive DNA-replication including complete characterization of an exonuclease-deficient mutant. Biochemistry 30:511–525.
39. Johnson KA (2010) The kinetic and chemical mechanism of high-fidelity DNA polymerases. Biochim Biophys Acta 1804:1041–1048.
40. Goulian M, Lucas ZJ, Kornberg A (1968) Enzymatic synthesis of deoxyribonucleic acid .25. Purification and properties of deoxyribonucleic acid polymerase induced by infection with phage T4. J Biol Chem 243:627–638.
41. Bakhtina M, Lee S, Wang Y, Dunlap C, Lamarche B, Tsai MD (2005) Use of viscogens, dNTP-alpha-S, and rhodium(III) as probes in stopped-flow, experiments to obtain new evidence for the mechanism of catalysis by DNA polymerase beta. Biochemistry 44:5177–5187.
42. Bermek O, Grindley NDF, Joyce CM (2011) Distinct roles of the active-site Mg^{2+} ligands, Asp(882) and Asp (705), of DNA polymerase I (Klenow fragment) during the prechemistry conformational transitions. J Biol Chem 286:3755–3766.